Light control of the nanoscale phase separation in heteroepitaxial nickelates

G. Mattoni,[1,*] N. Manca,[1] M. Hadjimichael,[2] P. Zubko,[2] A. J. H. van der Torren,[3] C. Yin,[3] S. Catalano,[4] M. Gibert,[4] F. Maccherozzi,[5] Y. Liu,[5] S. S. Dhesi,[5] and A. D. Caviglia[1]

[1]*Kavli Institute of Nanoscience, Delft University of Technology, 2628 CJ Delft, The Netherlands*

[2]*London Centre for Nanotechnology and Department of Physics and Astronomy, University College London, 17–19 Gordon Street, London WC1H 0AH, United Kingdom*

[3]*Kamerlingh Onnes-Huygens Laboratory, Leiden University, P.O. Box 9504, 2300 RA Leiden, The Netherlands*

[4]*Département de Physique de la Matière Quantique, University of Geneva, 24 Quai Ernest-Ansermet, 1211 Genève 4, Switzerland*

[5]*Diamond Light Source, Harwell Science and Innovation Campus, Didcot, Chilton, OX11 0DE, United Kingdom*

(Received 18 May 2018; revised manuscript received 17 July 2018; published 13 August 2018)

Strongly correlated materials show unique solid-state phase transitions with rich nanoscale phenomenology that can be controlled by external stimuli. Particularly interesting is the case of light–matter interaction in the proximity of the metal–insulator transition of heteroepitaxial nickelates. In this work, we use near-infrared laser light in the high-intensity excitation regime to manipulate the nanoscale phase separation in $NdNiO_3$. By tuning the laser intensity, we can reproducibly set the coverage of insulating nanodomains, which we image by photoemission electron microscopy, thus semipermanently configuring the material state. With the aid of transport measurements and finite element simulations, we identify two different timescales of thermal dynamics in the light–matter interaction: a steady-state and a fast transient local heating. These results open interesting perspectives for locally manipulating and reconfiguring electronic order at the nanoscale by optical means.

DOI: 10.1103/PhysRevMaterials.2.085002

I. INTRODUCTION

Rare-earth nickelates have received significant research attention, motivated by their unique properties that include a sharp metal–insulator transition (MIT) and unusual magnetic order [1,2]. The microscopic origin of these phenomena is still intensely studied and various models of charge localization are being considered in light of a bond disproportionated insulating state observed in experiments [3–10]. Independently of the exact microscopic picture, it is clear that these materials are characterized by a delicate balance between lattice distortions, covalency, and electronic correlations [11–15]. This leads to a remarkable tunability of the MIT with chemical and static pressure, epitaxial strain, heterointerfaces, and even near- or midinfrared light excitation [16–23]. From this perspective, the case of light–matter interaction is particularly interesting. For near-infrared charge excitations it was demonstrated that the system shows an ultrafast demagnetisation process driven by a photoexcited electronic mechanism [24–26]. Only at high excitation intensities an energy redistribution to the lattice becomes apparent. Since heteroepitaxial nickelates show rich nanoscale physics, including phase separation at the MIT, there is an increasing interest to explore the effects of light excitation on the domain structure [27–29]. Furthermore, ultrashort light pulses offer the unique possibility of providing energy with high intensity to localised regions of a material, allowing us to engineer the physical properties at the local scale.

In this work, we perform high-intensity laser excitations in the vicinity of the MIT of $NdNiO_3$ thin films, while imaging the nanoscale phase separation with photoemission electron microscopy (PEEM). We show that, by tuning the intensity of a near-infrared ultrafast laser, the equilibrium properties of heteroepitaxial nickelates can be controlled in two ways. First, different configurations of surface insulating nanodomains can be reproducibly realized. Second, the sharpness and width of MIT hysteresis can be manipulated. We discuss the observed effects in the framework of the interplay between light–matter interaction, heat transfer, and localized temperature increments, supporting our findings with both resistive measurements and finite element simulations. Our results pave the way to using ultrashort laser pulses to control local phase transitions in strongly correlated materials.

II. RESULTS

A. Light effects on the MIT

The experiment is performed on a 25-unit-cell-thick (9.5 nm) $NdNiO_3$ (NNO) film grown on a (110) $NdGaO_3$ substrate. X-ray diffraction measurements indicate that the NNO has single crystal quality, and it is coherently strained to the substrate lattice (further details in the Supplemental Material [30]). Electrical transport characterization [30] shows the presence of a sharp resistive transition from a high-temperature metallic state to a low-temperature insulating state, in agreement with what is expected for high-quality NNO thin films [19,31,32]. The sample is irradiated with a pulsed laser source (140 fs pulse length, 800 nm wavelength, 25 kHz repetition rate) focused on a 80 μm × 100 μm spot. The laser photon energy (1.5 eV) matches a broad absorption peak of NNO, which has negligible temperature dependence within the range explored in the experiment [33]. We track the changes

*g.mattoni@tudelft.nl

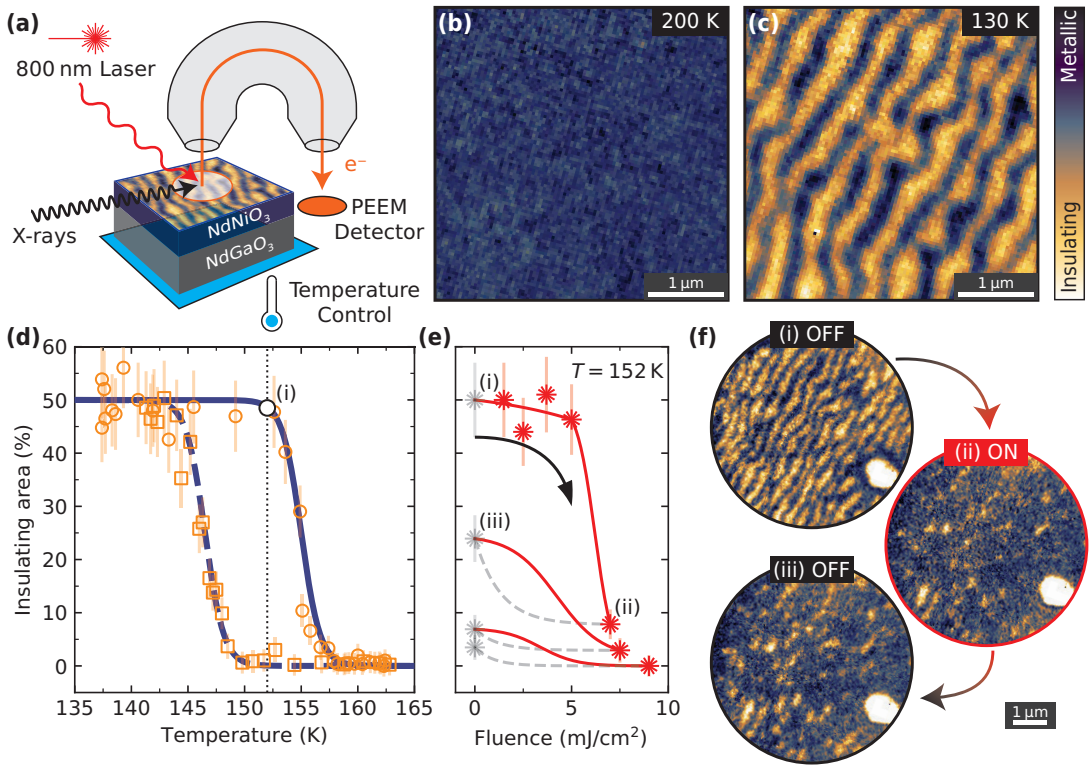

FIG. 1. MIT imaged by PEEM and controlled by light. (a) Schematic description of the experimental setup. (b) Homogeneous metallic state at 200 K and (c) striped insulating state at 130 K imaged by PEEM. (d) Hysteretic temperature dependence of the insulating domain coverage measured by PEEM upon cooling (squares) and warming (circles). The data is fitted with Eq. (1). (e) Effect of the laser light on the domain configuration at 152 K. The system is prepared with the laser off (grayed out symbol) in the state (i) indicated in (d), and laser light with different fluence (red symbols) is used to control the phase separation (solid and dashed lines are guides to the eye). (f) PEEM images corresponding to the states (i), (ii), and (iii) indicated in (e).

induced by optical excitation by imaging the spatial distribution of metallic and insulating areas with PEEM, as sketched in Fig. 1(a). Our imaging contrast is based on the different Ni L_3 x-ray absorption in the metallic and insulating phases, which in this case peak at 852.7 and 853.4 eV, respectively, as detailed in Ref. [29]. The sample is mounted on a cold finger, allowing controlled heating and cooling between 130 and 300 K. At 200 K, above the MIT, we find a homogeneous metallic phase [Fig. 1(b)], while at 130 K, right below the MIT, the material is in a mixed-phase state [Fig. 1(c)], with coexistence of insulating and metallic regions. Their striped shape is determined by the step and terrace surface morphology imposed by the substrate, as confirmed by topographic images acquired by atomic force microscopy [30]. As discussed in our previous work [29], the PEEM technique probes only the phase-separation occurring on the material surface, which typically has a slightly different transition temperature with respect to the bulk.

Figure 1(d) shows the temperature evolution of the insulating domains during a cycle of cooling (squares) and warming (circles) while the laser is off. Each data point is calculated from a single PEEM image as discussed in the Supplemental Material [30]. The data shows the typical hysteresis of NNO phase transition, where the insulating area increases upon cooling from 0% to a saturation coverage of 50%. This temperature dependence is well described by two sigmoid functions, representing the ramps of cooling (dashed) and warming (solid), with equation

$$A_{\mathrm{ins}}(T) = \frac{A_{\mathrm{ins}}^{\max}}{1 + e^{-w_i(T-T_i)}}, \tag{1}$$

where $A_{\mathrm{ins}}^{\max} = 50\%$ is the maximum area covered by the insulating phase and w_i, T_i are fitting parameters. In this case, we find $T_{\mathrm{MI}} = 146\,\mathrm{K}$ and $T_{\mathrm{IM}} = 155\,\mathrm{K}$, which determine the hysteresis width $\Delta T_{\mathrm{MIT}} = 9\,\mathrm{K}$.

To study the effects of the optical excitation we start with the laser off and set the thermal bath at 152 K by heating the sample from base temperature. This initial state (i) lies on the upper branch of the hysteresis loop and corresponds to a saturated insulating phase, as indicated in Fig. 1(e) and shown by the corresponding PEEM image in Fig. 1(f). The size of the region measured by PEEM ($5\,\mu\mathrm{m} \times 5\,\mu\mathrm{m}$) is much smaller than the laser light spot, ensuring the probing of a homogeneously excited region. We acquire a series of PEEM images for different values of laser fluence Φ and report the resulting coverage of insulating domains in Fig. 1(e). The images represent a steady-state condition of the system because the acquisition of a single PEEM measurement requires about 30 s of integration time, a time scale much longer than the 40 μs laser repetition period. An example of the effect of the laser excitation on the domain structure is shown in Fig. 1(f), where the laser fluence $\Phi = 7\,\mathrm{mJ\,cm^{-2}}$ reduces the insulating domain coverage A_{ins} from 50% to about 10%, leaving on the surface a few disconnected insulating regions in the state (ii).

Upon turning the laser off, A_{ins} does not recover to its initial value, but settles to an intermediate coverage of 25% shown in the state (iii). This partial recovery is a consequence of the hysteretic nature of the NNO phase transition, which keeps memory of the laser excitation as will be discussed below.

The process described above is fully reproducible and the final coverage is set by the laser fluence. The data in Fig. 1(e) shows that, by increasing the laser fluence, it is possible to gradually reduce A_{ins} down to a complete suppression of the insulating domain coverage with $\Phi = 9\,\mathrm{mJ\,cm^{-2}}$ at 152 K. Upon switching the laser off, a few insulating patches reappear also in this case. This insulating domain configuration is stable over time and the initial condition can be restored by cooling the sample below T_{MI}. In the following, we argue that the dominant mechanism for the laser control of the domain configuration can be attributed to thermal effects. A first indication of this comes from the threshold behavior observed in the fluence dependence in Fig. 1(e) where a reduction of A_{ins} is observed only for fluence $\Phi > 5\,\mathrm{mJ\,cm^{-2}}$. Previous reports indicated that, below this threshold, ultrafast photoexcitation in nickelates determines an ultrafast dynamics that can lead to a complete melting of the low temperature insulating phase [24,25]. Thermal effects were shown to take place in the higher excitation regime, involving energy redistribution to the crystal lattice, a phenomenology which we investigate in this work.

B. MIT cycles with photoexcitation

A first insight into the light control mechanism of the insulating domains of NNO is obtained by measuring the temperature dependence of A_{ins} for different fixed laser fluences. To this purpose, we acquired a series of PEEM spectroscopic maps under pulsed laser irradiation at different bath temperatures. Before cycling the temperature we reach a steady-state condition by maintaining a constant laser fluence Φ for several minutes at $T = 170\,\mathrm{K}$. Each cycle presents a hysteresis loop for A_{ins}, shown by the cooling (dashed) and warming (solid) curves in Fig. 2(a) (raw data in the Supplemental Material [30]). Upon increasing Φ, the hysteresis loop changes in two ways: It shifts to lower temperatures and it shrinks in width. These effects are summarised in Fig. 2(b), where the values of T_{MI} (squares) and T_{IM} (circles) are shown as a function of Φ. Both temperatures have a decreasing trend, but the slope of T_{MI} is smaller, resulting in a decrease of the hysteresis width ΔT_{MIT} [Fig. 2(c)]. A linear extrapolation also suggests that $\Delta T_{MIT} \sim 0$ at about $\Phi = 20\,\mathrm{mJ\,cm^{-2}}$, indicating that the MIT hysteresis can be fully suppressed by high intensity laser light. The reduction of the hysteresis width cannot be explained by a steady-state increase of the sample temperature because that would lead to identical changes of both T_{MI} and T_{IM}, thus rigidly shifting the hysteresis loop to lower temperature. In the following, we show that changes in ΔT_{MIT} stem from the MIT memory effect and that they can be explained by considering the detailed temporal evolution of the material temperature.

C. Transient heating by transport

We consider the effects of a transient heating on the NNO phase transition by studying selected warming and cooling cycles. Inside the MIT hysteresis window it is possible to perform

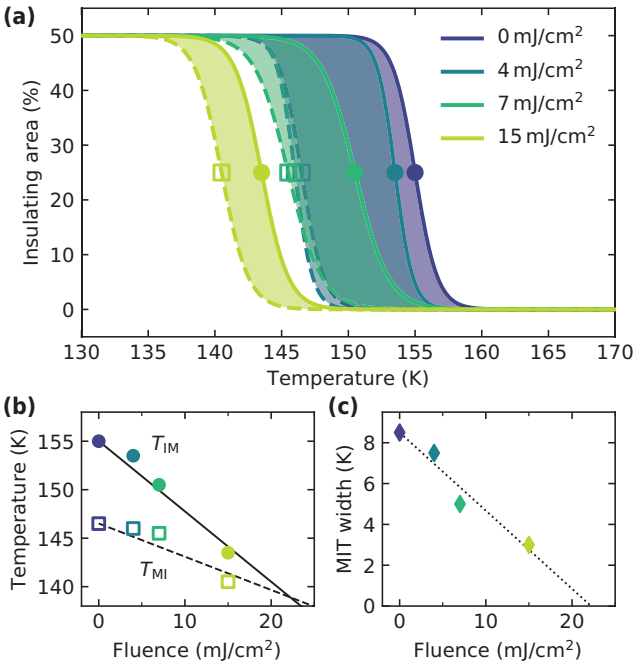

FIG. 2. MIT hysteresis with different laser fluence. (a) Change of the PEEM hysteresis loop with different laser fluence. (b) T_{IM} (circles), T_{MI} (squares), and (c) ΔT_{MIT} extracted from the sigmoid fit. The lines are linear regressions of the data.

nested loops by sweeping the temperature over a range that is narrower than the full hysteresis width. We carry out electrical transport measurements to monitor the sample resistivity while slowly varying the temperature at a rate of $0.5\,\mathrm{K\,min^{-1}}$, thus preserving a quasistatic condition. We note that because this analysis probes properties intrinsic to hysteretic MITs our results apply both to the bulk and the surface domain structure. We present the resistance versus temperature characteristic in Fig. 3, where the black lines show the full hysteresis loop, with the lower branch relative to cooling (dashed line) and the upper branch relative to warming (solid line). For comparison with the PEEM data in Fig. 2, the thermal bath is initially fixed to the middle of the hysteresis at $T_0 = 155\,\mathrm{K}$ (vertical dotted line). This value is reached by starting from base temperature, to set the sample into a state on the upper branch, with maximum coverage of insulating domains. Nested loops are then measured by increasing the temperature of an amount ΔT and then bringing it back to T_0. At the end of the loop the sample resistance at T_0 [circles in Fig. 3(a)] remains approximately constant for $\Delta T \leqslant 8\,\mathrm{K}$, after which it decreases monotonously and reaches the lower hysteresis branch for $\Delta T \sim 20\,\mathrm{K}$. At this point the insulating domains have turned metallic and no further change is observed. The lower branch, in fact, is the minimum resistivity curve that can be reached in the hysteresis region. We now repeat the experiment starting from a state on the lower branch [Fig. 3(b)], which is obtained by cooling to $T_0 = 150\,\mathrm{K}$ starting from room temperature. Performing nested loops we find that all the end points, marked as squares, lie on top of each other.

This analysis shows that if the system is probed at a certain T_0 after a transient temperature increase ΔT, the domain

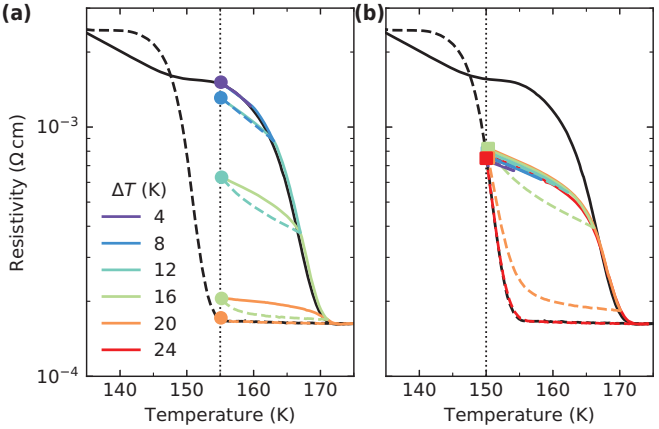

FIG. 3. Nested MIT cycles measured by electrical transport. Warming–cooling loops of width ΔT obtained starting from (a) the upper branch of the hysteresis loop at $T_0 = 155$ K and (b) the lower branch at $T_0 = 150$ K. The end point of each nested cycle is indicated by a dot or a square.

population is not affected if the initial state is on the lower hysteresis branch. The behavior is similar to what is observed in other oxides characterized by hysteretic MIT [34–36], and explains how a transient temperature spike, as the one induced by the laser pump, can shrink the hysteresis width as observed in Fig. 2. Most of the heat transferred by a laser pulse is, in fact, dissipated in a time scale faster than the laser repetition period of 40 μs, so that the material experiences transient temperature spikes on top of a steady-state temperature raise. Because PEEM measurements average the surface state over 30 s, the transient temperature spike shifts the upper branch of the hysteresis loop to lower temperature, while it does not affect the lower branch. This effect is responsible for the reduction of ΔT_{MIT} that we observed in the PEEM data. Conversely, the shift of the lower branch should be related to a steady-state temperature rise determined by the average incident light power. Since it is not possible to access the transient heating dynamics in our experimental configuration, we qualitatively study the thermal response of the NNO material using classical heat transfer theory.

D. Laser heating simulation

We model the interaction of the laser with the sample by considering its heating implications through a finite element simulation. The geometry of the system is schematically illustrated in Fig. 4(a). We use a Gaussian time profile to describe the laser excitation [Fig. 4(b)]. We calculate the heat transferred to the lattice with a linear response function with characteristic time $\tau = 100$ ps and we use it as the input power for our simulation (details in the Supplemental Material [30]). This model allows us to focus directly on the energy redistribution to the crystal lattice and neglect ultrafast dynamics of the system, which occur on shorter time scales [24]. In the initial conditions the system is in equilibrium with a thermal bath at 150 K [state (i) of Figs. 4(c) and 4(d)]. Since the light absorption coefficient is much larger in the film rather than in the substrate ($\alpha_{\mathrm{NNO}} \gg \alpha_{\mathrm{NdGaO_3}}$), the former absorbs the input power with higher density, determining a sharp temperature rise, which peaks at $t = 100$ ps [state (ii)]. After 1 ns [state (iii)] most of this heat has diffused into the colder substrate. The same temperature spike $\Delta T_{\mathrm{transient}}$ is observed for each laser pulse. Because of the slow heat dissipation toward the thermal bath, residual heat is retained at the arrival of the following laser pulse ($t = 40\,\mu$s). After multiple pulses, the residual heat determines a steady-state temperature rise $\Delta T_{\mathrm{steadystate}}$. These two temperature variations are indicated by arrows in Fig. 4(d), where the simulation is performed with a laser fluence $\Phi = 1$ mJ cm^{-2}. We show in Figs. 4(e) and 4(f) that both $\Delta T_{\mathrm{transient}}$ and $\Delta T_{\mathrm{steadystate}}$ increase linearly with Φ.

In accordance with the analysis carried out in Fig. 3, we identify the transient spike as responsible for the shrinking of the MIT hysteresis ($\Delta T_{\mathrm{transient}}(\Phi) \sim [\Delta T_{\mathrm{MIT}}(\Phi) - \Delta T_{\mathrm{MIT}}(0)]$), while the steady-state rise is responsible for the shift of the whole hysteresis loop to lower temperatures ($\Delta T_{\mathrm{steadystate}}(\Phi) \sim [T_{\mathrm{MI}}(\Phi) - T_{\mathrm{MI}}(0)]$). In Figs. 4(e) and 4(f) we compare our experimental data with the simulation results. The curves show similar trends, with $\Delta T_{\mathrm{transient}}(\Phi)$ and $\Delta T_{\mathrm{steadystate}}(\Phi)$ linearly increasing as a function of laser fluence. However, the experimental and simulated slopes differ by a factor of about 3, indicating that our finite element model does not achieve a quantitative description of the NNO response. A possible explanation for this discrepancy is an underestimation of the material reflectivity [30], responsible for a lower laser power absorbed in the low-angle geometry used in our experiment. In addition, our model is based on a linear optical response, while in the considered regime of high laser fluence the absorption might become saturated, reducing the effective value of α_{NNO} [30]. Another source of uncertainty is the value of the linear response relaxation time $\tau = 100$ ps that we used in the simulation [30]. Finally, additional heat dissipation effects that are not included in our model might also affect the system thermal response. Although these different sources of uncertainty prevent an accurate quantitative description, our simulations indicate that a dual transient and steady-state temperature rise is intrinsic to this experiment, and is observed for all realistic combinations of the simulation parameters (for an extended discussion see the Supplemental Material [30]). The calculated temperature dynamics is in good agreement with the PEEM data of insulating and metallic domains, making our analysis a consistent description of the experimental results.

III. CONCLUSIONS

To conclude, we have shown how ultra-fast laser radiation in the high-intensity excitation regime can be used to control the phase transition in nickelates. By tuning the laser fluence, we were able to manipulate the equilibrium properties of the material and semipermanently configure the coverage of insulating nanodomains. With the aid of electrical transport measurements and finite element simulations, we identified thermal effects on two different time scales to be the driving mechanism for the achieved light control. Our results show how ultrafast laser pulses can be used to selectively regulate nanoscale order in strongly correlated materials, opening new possibilities for controlling phase transitions at the local level.

ACKNOWLEDGMENTS

We thank Diamond Light Source for access to beamtime under Proposals No. SI-13081 and No. SI-10428. This work

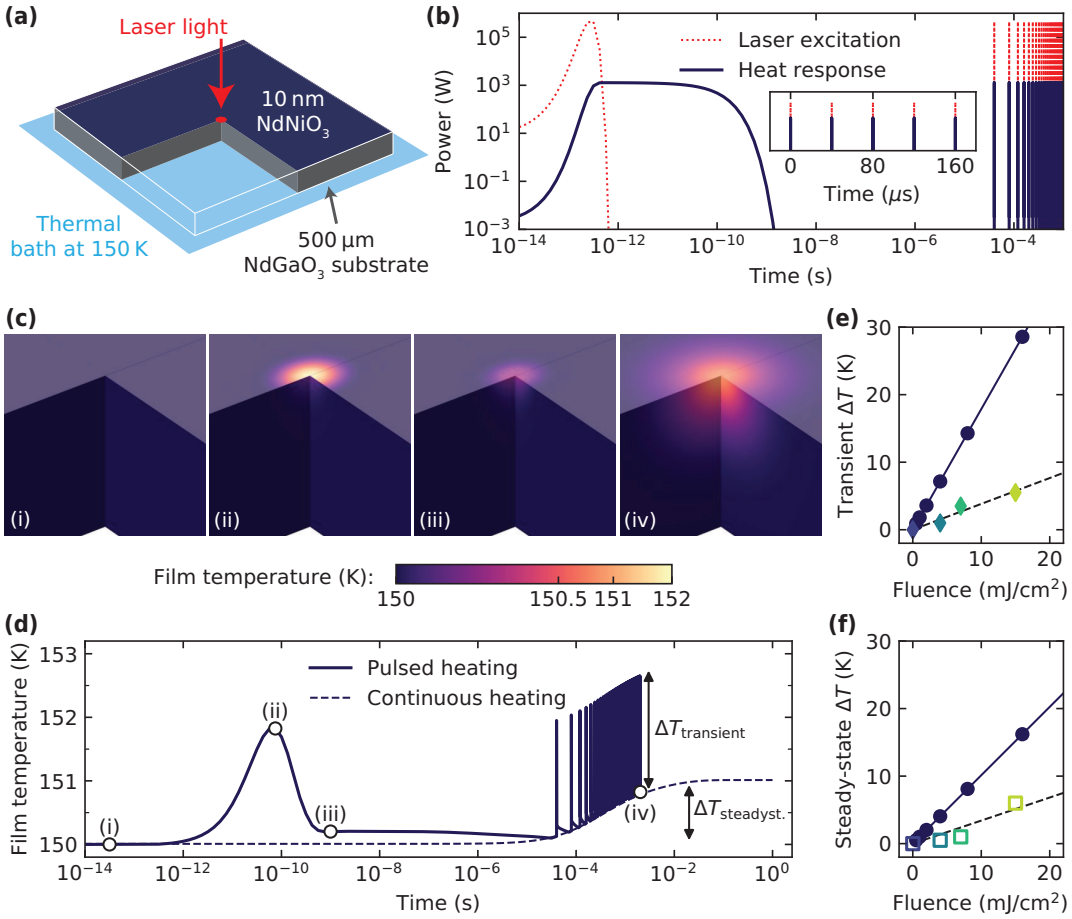

FIG. 4. Laser heating model based on finite elements analysis. (a) Simulated geometry: The substrate is in thermal contact with a thermal bath at 150 K and the input power (laser pulse) is incident on a circular area on the top surface (further details in Supplementary Information). (b) Input laser power (red dotted line) and the corresponding heat response of the system (blue solid line) as a function of time on a logarithmic scale, with model parameters $\tau = 100$ ps and $\Phi = 1$ mJ cm^{-2}. The inset shows the same plot on a linear scale. (c) Temperature map at $t =$ (i) 100 fs, (ii) 100 ps, (iii) 1 ns, and (iv) 2 ms. (d) NNO surface temperature in the center of the laser spot as a function of time. Point (ii) marks a transient temperature spike $\Delta T_{\text{transient}}$ after each laser pulse, whereas the overall steady-state increase in temperature $\Delta T_{\text{steadystate}}$ is shown by the arrows at longer time scale. (e) Simulated transient and (f) steady-state temperature increase as a function of laser fluence (blue circles) compared to the experimental data (diamonds and squares) of Figs. 2(b) and 2(c).

was supported by The Netherlands Organisation for Scientific Research (NWO/OCW) as part of the Frontiers of Nanoscience program (NanoFront), by the Dutch Foundation for Fundamental Research on Matter (FOM). The research leading to these results has received funding from the European Research Council under the European Union's H2020 programme/ERC Grant Agreement No. 677458 (A.D.C.), EPSRC Grants No. EP/M007073/1 and No. 1447654.

[1] M. L. Medarde, J. Phys.: Condens. Matter **9**, 1679 (1997).
[2] G. Catalan, Phase Transit. **81**, 729 (2008).
[3] T. Mizokawa, D. I. Khomskii, and G. A. Sawatzky, Phys. Rev. B **61**, 11263 (2000).
[4] V. Scagnoli, U. Staub, Y. Bodenthin, M. Garcia-Fernandez, A. M. Mulders, G. I. Meijer, and G. Hammerl, Phys. Rev. B **77**, 115138 (2008).
[5] J. Liu, S. Okamoto, M. van Veenendaal, M. Kareev, B. Gray, P. Ryan, J. W. Freeland, and J. Chakhalian, Phys. Rev. B **83**, 161102(R) (2011).
[6] S. B. Lee, R. Chen, and L. Balents, Phys. Rev. B **84**, 165119 (2011).
[7] H. Park, A. J. Millis, and C. A. Marianetti, Phys. Rev. Lett. **109**, 156402 (2012).
[8] M. H. Upton, Y. Choi, H. Park, J. Liu, D. Meyers, J. Chakhalian, S. Middey, J.-W. Kim, and P. J. Ryan, Phys. Rev. Lett. **115**, 036401 (2015).
[9] A. Subedi, O. E. Peil, and A. Georges, Phys. Rev. B **91**, 075128 (2015).
[10] V. Bisogni, S. Catalano, R. J. Green, M. Gibert, R. Scherwitzl, Y. Huang, V. N. Strocov, P. Zubko, S. Balandeh, J.-M. Triscone *et al.*, Nat. Commun. **7**, 13017 (2016).
[11] M. Gibert, P. Zubko, R. Scherwitzl, J. Íñiguez, and J.-M. Triscone, Nat. Mater. **11**, 195 (2012).

[12] D. P. Kumah, A. S. Disa, J. H. Ngai, H. Chen, A. Malashevich, J. W. Reiner, S. Ismail-Beigi, F. J. Walker, and C. H. Ahn, Adv. Mater. **26**, 1935 (2014).
[13] A. J. Hauser, E. Mikheev, N. E. Moreno, J. Hwang, J. Y. Zhang, and S. Stemmer, Appl. Phys. Lett. **106**, 092104 (2015).
[14] M. N. Grisolia, J. Varignon, G. Sanchez-Santolino, A. Arora, S. Valencia, M. Varela, R. Abrudan, E. Weschke, E. Schierle, J. E. Rault *et al.*, Nat. Phys. **12**, 484 (2016).
[15] J. Fowlie, M. Gibert, G. Tieri, A. Gloter, J. Íñiguez, A. Filippetti, S. Catalano, S. Gariglio, A. Schober, M. Guennou *et al.*, Adv. Mater. **29**, 1605197 (2017).
[16] X. Obradors, L. M. Paulius, M. B. Maple, J. B. Torrance, A. I. Nazzal, J. Fontcuberta, and X. Granados, Phys. Rev. B **47**, 12353 (1993).
[17] P. C. Canfield, J. D. Thompson, S. W. Cheong, and L. W. Rupp, Phys. Rev. B **47**, 12357 (1993).
[18] A. Tiwari, C. Jin, and J. Narayan, Appl. Phys. Lett. **80**, 4039 (2002).
[19] R. Scherwitzl, P. Zubko, I. G. Lezama, S. Ono, A. F. Morpurgo, G. Catalan, and J.-M. Triscone, Adv. Mater. **22**, 5517 (2010).
[20] A. V. Boris, Y. Matiks, E. Benckiser, A. Frano, P. Popovich, V. Hinkov, P. Wochner, M. Castro-Colin, E. Detemple, V. K. Malik *et al.*, Science **332**, 937 (2011).
[21] G. Berner, M. Sing, F. Pfaff, E. Benckiser, M. Wu, G. Christiani, G. Logvenov, H.-U. Habermeier, M. Kobayashi, V. N. Strocov *et al.*, Phys. Rev. B **92**, 125130 (2015).
[22] A. D. Caviglia, R. Scherwitzl, P. Popovich, W. Hu, H. Bromberger, R. Singla, M. Mitrano, M. C. Hoffmann, S. Kaiser, P. Zubko *et al.*, Phys. Rev. Lett. **108**, 136801 (2012).
[23] M. Forst, A. D. Caviglia, R. Scherwitzl, R. Mankowsky, P. Zubko, V. Khanna, H. Bromberger, S. B. Wilkins, Y.-D. Chuang, W. S. Lee, W. F. Schlotter, J. J. Turner, G. L. Dakovski, M. P. Minitti, J. Robinson, S. R. Clark, D. Jaksch, J.-M. Triscone, J. P. Hill, S. S. Dhesi, and A. Cavalleri, Nat. Mater. **14**, 883 (2015).
[24] A. D. Caviglia, M. Först, R. Scherwitzl, V. Khanna, H. Bromberger, R. Mankowsky, R. Singla, Y.-D. Chuang, W. S. Lee, O. Krupin *et al.*, Phys. Rev. B **88**, 220401 (2013).
[25] P. Ruello, S. Zhang, P. Laffez, B. Perrin, and V. Gusev, Phys. Rev. B **76**, 165107 (2007).
[26] M. Först, K. R. Beyerlein, R. Mankowsky, W. Hu, G. Mattoni, S. Catalano, M. Gibert, O. Yefanov, J. N. Clark, A. Frano *et al.*, Phys. Rev. Lett. **118**, 027401 (2017).
[27] G. Catalan, R. M. Bowman, and J. M. Gregg, Phys. Rev. B **62**, 7892 (2000).
[28] D. Kumar, K. P. Rajeev, A. K. Kushwaha, and R. C. Budhani, J. Appl. Phys. **108**, 063503 (2010).
[29] G. Mattoni, P. Zubko, F. Maccherozzi, A. J. H. van der Torren, D. B. Boltje, M. Hadjimichael, N. Manca, S. Catalano, M. Gibert, Y. Liu *et al.*, Nat. Commun. **7**, 13141 (2016).
[30] See Supplemental Material at http://link.aps.org/supplemental/10.1103/PhysRevMaterials.2.085002 for additional information on the film structural characterization, electrical transport measurements, raw PEEM data, laser heating model and material parameters used for the simulation, additional simulation data, which includes Refs. [37–39].
[31] X. Granados, J. Fontcuberta, X. Obradors, L. Manosa, and J. B. Torrance, Phys. Rev. B **48**, 11666 (1993).
[32] S. Catalano, M. Gibert, V. Bisogni, F. He, R. Sutarto, M. Viret, P. Zubko, R. Scherwitzl, G. A. Sawatzky, T. Schmitt *et al.*, APL Mater. **3**, 062506 (2015).
[33] J. Ruppen, J. Teyssier, I. Ardizzone, O. E. Peil, S. Catalano, M. Gibert, J.-M. Triscone, A. Georges, and D. van der Marel, Phys. Rev. B **96**, 045120 (2017).
[34] J.-G. Ramírez, A. Sharoni, Y. Dubi, M. E. Gómez, and I. K. Schuller, Phys. Rev. B **79**, 235110 (2009).
[35] L. Pellegrino, N. Manca, T. Kanki, H. Tanaka, M. Biasotti, E. Bellingeri, A. S. Siri, and D. Marré, Adv. Mater. **24**, 2929 (2012).
[36] V. Franco, F. Béron, K. R. Pirota, M. Knobel, and M. A. Willard, J. Appl. Phys. **117**, 17C124 (2015).
[37] V. M. Orera, L. E. Trinkler, R. I. Merino, and A. Larrea, J. Phys.: Condens. Matter **7**, 9657 (1995).
[38] W. Schnelle, R. Fischer, and E. Gmelin, J. Phys. D: Appl. Phys. **34**, 846 (2001).
[39] M. K. Hooda and C. S. Yadav, Physica B: Condens. Matter **491**, 31 (2016).